Tesla and a standard gadolinium chelate using a rat brain tumor model. Invest Radiol 2006;41:244–8.
6. Chappell PM, Pelc NJ, Foo TK, Glover GH, Haros SP, Enzmann DR. Comparison of lesion enhancement on spin-echo and gradient-echo images. Am J Neuroradiol 1994;15:37–44.
7. Rand S, Maravilla KR, Schmiedl U. Lesion enhancement in radio-frequency spoiled gradient-echo imaging: theory, experimental evaluation, and clinical implications. Am J Neuroradiol 1994;15:27–35.
8. Pui MH, Fok EC. MR imaging of the brain: comparison of gradient-echo and spin-echo pulse sequences. Am J Roentgenol 1995;165:959–62.
9. Fellner F, Holl K, Held P, Fellner C, Schmitt R, Bohm-Jurkovic H. A T1-weighted rapid three-dimensional gradient-echo technique (MP-RAGE) in preoperative MRI of intracranial tumours. Neuroradiology 1996;38: 199–206.
10. Li D, Haacke EM, Tarr RW, Venkatesan R, Lin W, Wielopolski P. Magnetic resonance imaging of the brain with gadopentetate dimeglumine-DTPA: comparison of T1-weighted spin-echo and 3D gradient-echo sequences. J Magn Reson Imaging 1996;6:415–24.
11. Elster AD. How much contrast is enough? Dependence of enhancement on field strength and MR pulse sequence. Eur Radiol 1997;7 Suppl 5:276–80.
12. Fischbach F, Bruhn H, Pech M, Neumann F, Ricke J, Felix R, et al. Efficacy of contrast medium use for neuroimaging at 3.0 T: utility of IR-FSE compared to other T1-weighted pulse sequences. J Comput Assist Tomogr 2005;29:499–505.
13. Raila FA, Bowles AP Jr, Perkins E, Terrell A. Sequential imaging and volumetric analysis of an intracerebral C6 glioma by means of a clinical MRI system. J Neurooncol 1999;43:11–7.
14. Thorsen F, Ersland L, Nordli H, Enger PO, Huszthy PC, Lundervold A, et al. Imaging of experimental rat gliomas using a clinical MR scanner. J Neurooncol 2003;63:225–31.
15. Blanchard J, Mathieu D, Patenaude Y, Fortin D. MR-pathological comparison in F98-Fischer glioma model using a human gantry. Can J Neurol Sci 2006;33: 86–91.
16. Wansapura JP, Holland SK, Dunn RS, Ball WS Jr. NMR relaxation times in the human brain at 3.0 tesla. J Magn Reson Imaging 1999;9:531–8.

Acta Radiologica **rad134548.3d** 23/10/07 20:33:45
The Charlesworth Group, Wakefield +44(0)1924 369598 - Rev 7.51n/W (Jan 20 2003)
262880

Eur J Nucl Med Mol Imaging
DOI 10.1007/s00259-007-0654-4

ORIGINAL ARTICLE

Absolute quantitation of myocardial blood flow with ^{201}Tl and dynamic SPECT in canine: optimisation and validation of kinetic modelling

Hidehiro Iida · Stefan Eberl · Kyeong-Min Kim · Yoshikazu Tamura · Yukihiko Ono · Mayumi Nakazawa · Antti Sohlberg · Tsutomu Zeniya · Takuya Hayashi · Hiroshi Watabe

Received: 18 September 2007 / Accepted: 4 November 2007

Abstract
Purpose ^{201}Tl has been extensively used for myocardial perfusion and viability assessment. Unlike ^{99m}Tc-labelled agents, such as ^{99m}Tc-sestamibi and ^{99m}Tc-tetrofosmine, the regional concentration of ^{201}Tl varies with time. This study is intended to validate a kinetic modelling approach for in vivo quantitative estimation of regional myocardial blood flow (MBF) and volume of distribution of ^{201}Tl using dynamic SPECT.
Methods Dynamic SPECT was carried out on 20 normal canines after the intravenous administration of ^{201}Tl using a commercial SPECT system. Seven animals were studied at rest, nine during adenosine infusion, and four after beta-blocker administration. Quantitative images were reconstructed with a previously validated technique, employing OS-EM with attenuation-correction, and transmission-dependent convolution subtraction scatter correction. Measured regional time–activity curves in myocardial segments were fitted to two- and three-compartment models. Regional MBF was defined as the influx rate constant (K_1) with corrections for the partial volume effect, haematocrit and limited first-pass extraction fraction, and was compared with that determined from radio-labelled microspheres experiments.
Results Regional time–activity curves responded well to pharmacological stress. Quantitative MBF values were higher with adenosine and decreased after beta-blocker compared to a resting condition. MBFs obtained with SPECT (MBF_{SPECT}) correlated well with the MBF values obtained by the radio-labelled microspheres (MBF_{MS}) ($MBF_{SPECT}=-0.067+1.042\times MBF_{MS}$, $p<0.001$). The three-compartment model provided better fit than the two-compartment model, but the difference in MBF values between the two methods was small and could be accounted for with a simple linear regression.
Conclusion Absolute quantitation of regional MBF, for a wide physiological flow range, appears to be feasible using ^{201}Tl and dynamic SPECT.

Keywords Myocardial blood flow · Dynamic SPECT · Thallium-201 · Compartment model · Quantitation

H. Iida (✉) · S. Eberl · K.-M. Kim · M. Nakazawa · A. Sohlberg · T. Zeniya · T. Hayashi · H. Watabe
Department of Investigative Radiology,
National Cardiovascular Center Research Institute,
Fujishiro-dai,
Suita City, Osaka 565-8565, Japan
e-mail: iida@ri.ncvc.go.jp

S. Eberl
PET and Nuclear Medicine Department,
Royal Prince Alfred Hospital,
Missenden Road,
Camperdown, NSW 2050, Australia

Y. Tamura
Department of Cardiology, Akita Kumiai General Hospital,
1-1-1, Nishi-bukuro, Iijima,
Akita City 011-0948, Japan

Y. Ono
Akita Research Institute of Brain,
6-10, Senshu-Kubota Machi,
Akita City 010-0874, Japan

Introduction

Myocardial perfusion imaging using Thallium-201 (^{201}Tl) is well established in routine clinical practice for detecting

exercise-induced myocardial ischaemia and/or for assessing myocardial viability in patients with coronary artery disease. The diagnosis, however, has been limited to qualitative or visual assessment of the physical extent of the defect areas rather than quantitative assessment of physiological functions. Quantitative methods would for example enable longitudinal studies when assessing therapy response and pharmacological interventions. Some groups have already investigated the feasibility of estimating quantitative parameters with dynamic SPECT in the myocardium using ^{201}Tl [1] and ^{99m}Tc-Teboroxime [1, 2], but these techniques have not yet been applied to clinical practice. This is largely attributed to the fact that quantitative reconstruction programmes are not readily available on commercial SPECT systems.

We have developed a reconstruction programme package for SPECT, which can accurately provide quantitative images of radio-labelled tracer distributions in vivo, which is a pre-requisite for absolute physiological parameter estimation. The adequacy and accuracy of these methods have been demonstrated in multiple papers for ^{99m}Tc and ^{201}Tl in cardiac studies [3–5], and for ^{99m}Tc and ^{123}I in brain studies [6]. It has also been demonstrated, in brain studies, that physiological parameters such as cerebral perfusion [6] and cerebral flow reactivity [7] obtained using our package were as accurate as those determined by PET. These findings suggest that absolute quantitation of regional myocardial perfusion might also be possible in a clinical setting using commercial SPECT cameras.

^{201}Tl is a potassium analogue, and its kinetics has been extensively investigated in previous studies [8, 9]. Due to the high first-pass extraction fraction (EF) [10] and a large distribution volume, ^{201}Tl has been considered an ideal tracer for quantitation of absolute myocardial blood flow, not only at rest but also at hyperemic conditions. As a clinical implication, quantitative assessment of MBF and coronary flow reserve is important. For instance, coronary microvascular dysfunction or impaired endothelial function in patients with coronary risk factors or patients with cardiomyopathy or with heart failure is an un-resolved important issue to answer [11]. Coronary flow reserve can also be reduced in patients with hyper-cholesterolemia without overt coronary stenosis [12]. The low energy and long half-life of ^{201}Tl have, however, seriously limited its use in nuclear cardiology.

The goal of this study was to validate our reconstruction methodology for the estimation of myocardial blood flow using ^{201}Tl and dynamic SPECT using tissue time–activity curves (TTAC) derived from myocardial regions. In addition, we aimed to find the optimal kinetic model configuration and to investigate the factors affecting the estimation of physiological parameters such as the partial volume effect (PVE), appropriate choice of input function, conversion from plasma to blood flow using haematocrit (Hct) and the limited first-pass tracer EF.

Materials and methods

Subjects

A total of 21 dogs were studied in which 8 were in a resting condition, 9 dogs during constant infusion of adenosine for increased MBF, and 4 dogs during constant infusion of beta-blocker. Of the 21 studies, 1 study was un-successful and projection data could not be retrieved from the scanner, reducing the number of resting studies to 7 and total dog studies to 20. Adenosine was infused continuously over the study duration at a rate ranging from 140 to 700 mg/kg/h to achieve a range of blood flow increases. An initial dose of beta-blockers ranging from 2 to 6 mg was given, followed by a constant infusion for the duration of the study of 2 or 4 mg/h. The study protocol was approved by the animal ethics committee at the Akita Research Institute of Brain, Akita City, Japan where all experiments were carried out.

SPECT procedures

All dogs were anaesthetised, and the catheters for dose administration and arterial blood sampling were inserted before the study. The SPECT system was a conventional dual-head gamma camera (Toshiba GCA-7200A, Tokyo, Japan) fitted with short focal length fan-beam collimators (LEHR-Fan). The transverse field-of-view (FOV) was 22 cm diameter and axial FOV was 20 cm. The dogs were carefully taped into a cradle to minimise motion during the study, and also to ensure that no truncation occurred. Heart rate and blood pressure were monitored throughout the study and recorded at regular intervals.

Before the injection of any tracer, a 15-min transmission study was carried out in which a rod source filled with approximately 740 MBq of ^{99m}Tc was placed along the focal line of one of the fan-beam collimators (see Fig. 1). The transmission study was followed by injection of 3 MBq of ^{141}Ce microspheres into the left ventricle via a catheter and blood was withdrawn from the aorta at a constant flow rate of 5 ml/min for 2 min to serve as an input function. For the pharmacological intervention studies, adenosine infusion or beta-blocker injection followed by infusion was commenced before the ^{141}Ce microsphere administration.

Dynamic SPECT was commenced with the start of the 4-min constant infusion of 110 MBq ^{201}Tl. The frame collection rates and 360° rotation times were 10×1 min (rotation time 15 s), 6×2 min (30 s), 3×4 min (60 s) and 5×5 min (60 s) for the first hour for all studies. Resting blood flow studies had an additional 18×10 min (120 s) frames collected for a total study period over 4 h. The shorter total study time for the drug infusion studies was mandated by the difficulties in keeping the dogs stable with prolonged infusions of the drugs used. A 34% energy

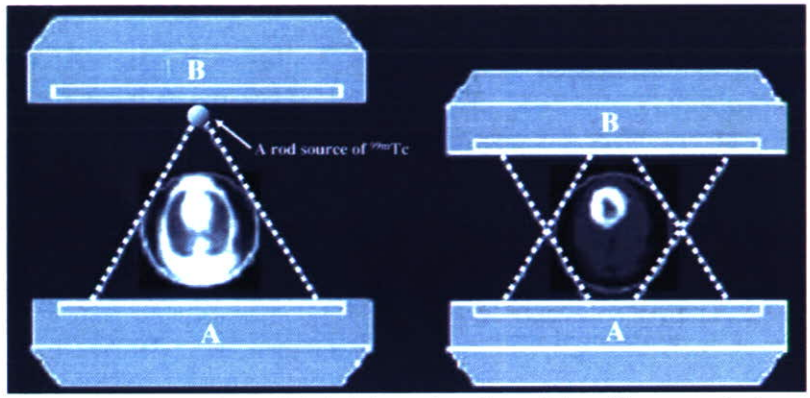

Fig. 1 Schematic diagram of data acquisition using a clinical dual-headed SPECT camera fitted with fan-beam collimators. Transmission scan was performed using a ^{99m}Tc-filled rod source placed at a focal line of one of the collimators, and only one of the detectors was used (*left*). Both detectors were used in the emission scan (*right*)

window centred on 77 keV was used for the ^{201}Tl acquisitions [4, 13].

Arterial blood samples were taken every 20 s for the first 6 min, every 60 s for 6–10 min, 120 s for 10–20 min, 300 s for 20–30 min and 600 s for 30–60 min. For the resting studies, blood samples were also taken every 20 min for 1–2 h and additional samples at 2.5, 3 and 4 h post-^{201}Tl infusion. In six studies, plasma was separated immediately after sampling by centrifugation, and plasma samples were counted in a well counter cross-calibrated with the SPECT scanner. To minimise the effects of the continued exchange of ^{201}Tl between plasma and red blood cells in the test tubes after sampling, immediate, rapid separation of plasma from whole blood was required. An averaged relationship between plasma and whole blood concentration ratio over time was obtained, and then multiplied with the whole blood curves for all studies to derive a plasma input function.

At the end of the SPECT study, the microsphere blood flow measurement was repeated with ^{51}Cr microspheres. The dogs were then killed by injection of potassium chloride (KCl) and the myocardium was dissected into samples suitable for counting in the well counter. The ^{201}Tl concentration in the tissue samples was derived from the sample weight normalised gamma counter counts. The samples were stored to allow for the decay of ^{201}Tl ($T_{1/2}$= 73 h vs $T_{1/2}$=32.5 days for ^{141}Ce and 27.8 days for ^{51}Cr) and then counted to measure the ^{141}Ce and ^{51}Cr activities. Separation between ^{141}Ce and ^{51}Cr counts was based on their respective gamma ray energies (145 keV for ^{141}Ce and 323 keV for ^{51}Cr).

SPECT data processing

Projection data were processed according to previously described procedures [5]. Briefly, the transmission data obtained by the fan-beam collimator were first re-binned into parallel projections. Transmission projections were normalised by blank projection, re-constructed to generate quantitative maps of the attenuation coefficient for ^{99m}Tc and then linearly scaled to provide attenuation correction maps for ^{201}Tl. Emission data were corrected for detector non-uniformity and also re-binned into parallel projections. The projection data were then corrected for scatter with transmission-dependent convolution subtraction (TDCS) originally proposed by Meikle et al. [14] and further optimised by our group [4, 5]. The emission projection data were re-constructed with the OS-EM reconstruction algorithm [15] using three iterations and ten subsets. The re-constructed images were cross-calibrated with the well counter system.

Data analysis

Re-constructed images were normalised by acquisition time for each frame. Multiple circular regions of interest (ROI) were drawn on the myocardium, and the TTAC of ^{201}Tl were generated for the anterior, apical, lateral, posterior and septal areas of the myocardium. The two-compartment model (one tissue compartment) and three-compartment model (two tissue compartments) shown in Fig. 2 were applied to determine two parameters (K_1 and K_2) for the two-compartment model and four parameters (K_1–K_4) for the three-compartment model by means of non-linear least squares fitting (NLLSF).

The regional MBF was considered to be related to K_1 obtained from compartment model fits. K_1 is, however, affected by the PVE, Hct and the limited first-pass EF whose effects were corrected according to Eq. 1:

$$\mathrm{MBF} = \frac{\mathrm{PVE}}{\mathrm{EF} \times (1 - \mathrm{Hct})} \times K_1 \qquad (1)$$

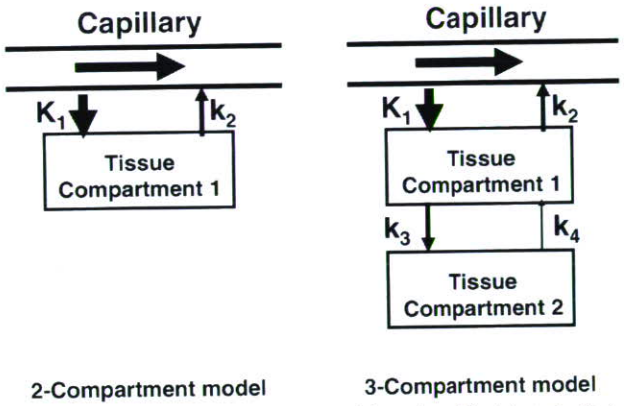

Fig. 2 Two- and three-compartment models evaluated in this study. K_1 in units of ml/min/g denotes the regional MBF for both models. Distribution volume (V_d) in units of ml/g is defined as K_1/k_2 for the two-compartment mode, and $\frac{K_1}{k_2}\left(1+\frac{k_3}{k_4}\right)$ for the three-compartment model

The physiological basis for the correction factors in Eq. 1 can be described as follows:

1. TTACs obtained from SPECT images are under-estimated due to the limited spatial resolution relative to the myocardial wall thickness and also due the myocardial contractile motion. This phenomenon is known as PVE. The PVE correction factor for each TTAC was determined from the ratio of the last SPECT frame counts to the ^{201}Tl myocardial tissue sample counts obtained from the tissue samples taken and measured with the well counter at the end of the SPECT scan.
2. The arterial input function for the compartment model studies was defined from the plasma radioactivity concentration curve, rather than the whole blood radioactivity curve. K_1 is therefore the regional "plasma" flow. Thus, for comparison with the microsphere flow measurements, which estimates the whole blood flow, K_1 was divided by (1−Hct) to obtain the flow for the total blood.
3. For a tracer with limited first-pass EF<1.0, flow (MBF) is related to K_1 by K_1=EF×MBF. The first-pass EF is flow-dependent and decreases at high flow. We have applied an empirical formulation for the first-pass EF based on the data by Weich et al. [10] (EF=0.84−0.524·$\log_{10}(K_1^*)$ where K_1^* is $K_1/(1-\text{Hct})$. The K_1 values obtained with two- and three-compartment models with/without corrections according to Eq. 1 were compared to the average of microsphere blood flow values obtained pre- and post-dynamic SPECT scan.

The distribution volume of ^{201}Tl (V_d) was defined as

$$V_d = \frac{K_1}{k_2} \text{ for the two} - \text{compartment model} \quad (2a)$$

$$V_d = \frac{K_1}{K_2}\left(1+\frac{K_3}{K_4}\right) \text{ for the three} - \text{compartment model.} \quad (2b)$$

As mentioned before, the resting studies were collected for 4 h, whilst the adenosine and beta-blocker studies were collected for approximately 1 h. To investigate whether the shorter collection time introduces systematic bias, NLLSF fits restricted to the first 1 h of the resting study data were also performed and compared with the V_d values from the full 4 h resting data set and with the estimates obtained from the beta-blocker and adenosine studies.

Akaike information criterion (AIC) and Schwarz criterion (SC) were calculated for both two-compartment and three-compartment model fits [16] to test the adequacy of the two models. All data are presented as mean±1 SD. Student's t test was employed in the comparison of the V_d values. Pearson's regression analysis was applied to compare K_1 and microsphere flow values. A probability value of <0.05 was considered statistically significant.

Results

Figure 3 shows the plasma to whole blood concentration ratios in the six dogs with rapid plasma separation and the averaged data. Equilibrium is reached after about 40 min, at which time the mean ratio was found to be 0.76. As expected, relative plasma concentration is highest early on as the tracer is injected into the plasma (and not red blood cells). ^{201}Tl is rapidly cleared from the plasma causing a rapid decline in relative plasma concentration and "undershoot" before equilibrium is established. Samples left for a prolonged period before plasma separation showed the value of approximately 0.78, which was close to the plasma to whole blood concentrations ratio at the equilibrium shown in

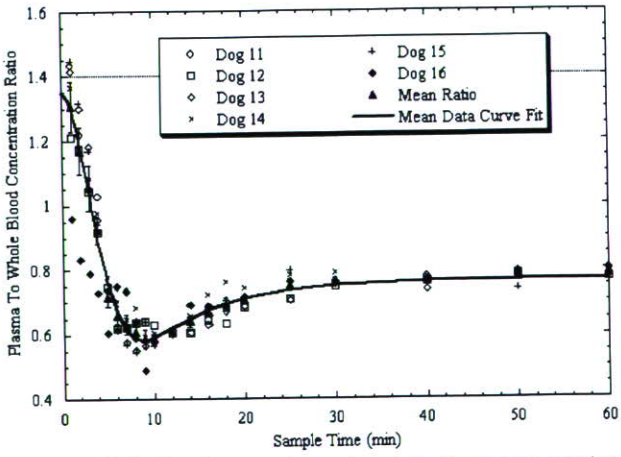

Fig. 3 Individual and mean plasma to whole blood concentration ratios over time for the six dogs with rapid plasma separation. *Error bars* indicate the standard error of the mean. *Solid line* is the curve fit to mean ratio data

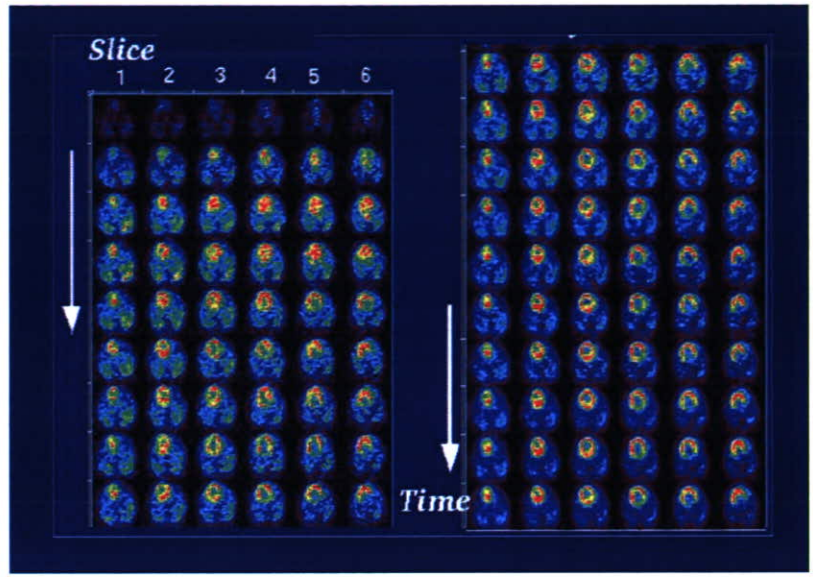

Fig. 4 A typical example of sequential SPECT images of the myocardium for six representative slices after intravenous injection of ^{201}Tl into a canine at rest

Fig. 3. The plasma to whole blood ratio curves could be approximated by the following equation:

$$R_{\mathrm{pl/wb}} = A_0 e^{-\lambda(t+\Delta t)^2} + A_1\left(1 - e^{-\lambda_2(t+\Delta t)}\right), \quad (3)$$

which resulted in A_0=1.303±0.045, A_1=0.7649±0.0056, λ_1=0.03636±0.0039 min^{-1}, λ_2=0.1263±0.0077 min^{-1} and Δt=0.9516±0.41 min. The correlation coefficient for the fit was r=0.995.

Figure 4 shows a typical example of sequential images after the intravenous injection of ^{201}Tl for six representative slices of a dog studied at rest. It can be seen that ^{201}Tl appeared in the ventricular chambers first and then gradually accumulated homogeneously into the left myocardium. The quality of these images is reasonably good, indicating that our approach of estimating the kinetic parameters by NLLSF is feasible without excessive noise

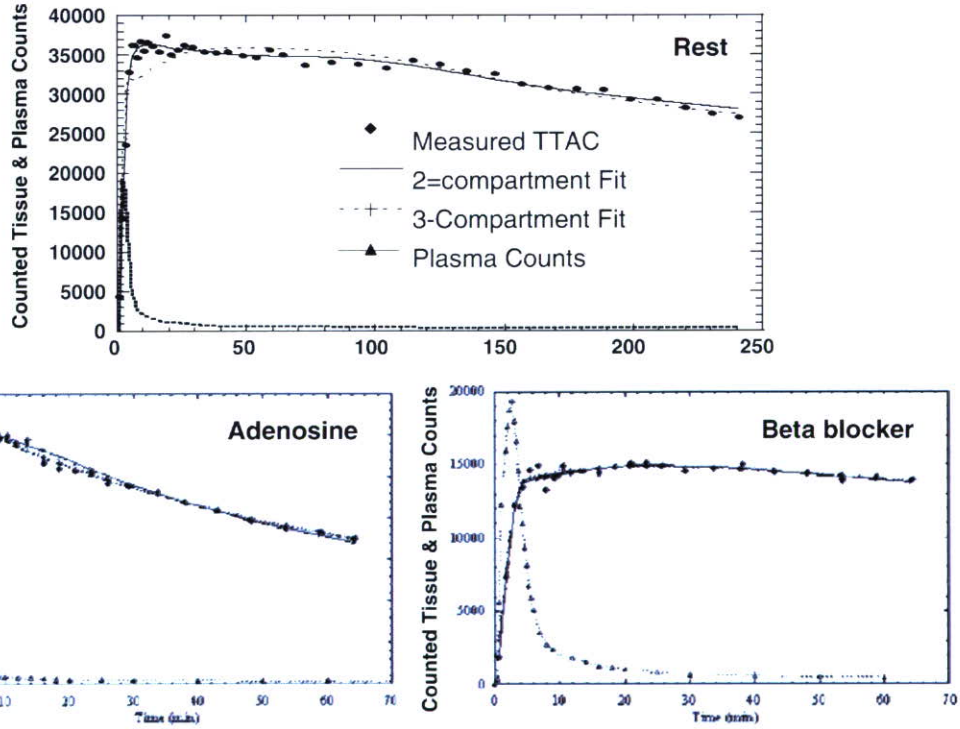

Fig. 5 TTACs and two- and three-compartment model fits for a resting, adenosine (increased MBF) and beta-blocker (reduced MBF) study. Note the different time scales for the resting study because resting studies were collected for 4 h compared to ≈1 h for the pharmacological intervention studies

amplification. Curve fits to representative TTACs for resting, beta-blocker and adenosine infusion studies are shown in Fig. 5. The height of the TTACs relative to the input function corresponded well with the pharmacological challenges. Compared to the resting studies, peaks of TTACs relative to the arterial input function were higher for adenosine and lower after beta-blocker administration. Results of kinetic fitting by the two- and three-compartment models are also plotted on this figure. Visually, the three-compartment model provided better fits than the two-compartment model to the observed TTACs, which is particularly evident for the initial scan period of the resting and adenosine studies.

Shown in Fig. 6a–e is the comparisons of K_1 obtained by NLLSF (three-compartment model fit) with the microsphere flow estimates. Values were averaged over the myocardial segments in both axes, thus each point corresponds to a single study. There was good correlation between K_1 and the microsphere flow when no corrections were applied, but K_1 significantly under-estimated the true flow (Fig. 6a). All the corrections improved the K_1 estimates (Fig. 6b–d) and the best agreement between K_1 and microsphere flow was observed when all three factors were corrected as described in Eq. 1 (Fig. 6e). Results of the regression analysis also demonstrated the highest correlation coefficient when all three correction factors were applied. Table 1 summarises the results of the Akaike information criteria (AIC) and Schwartz criteria (SC) obtained from the kinetic fitting analysis for all myocardial segments of all subjects. Both

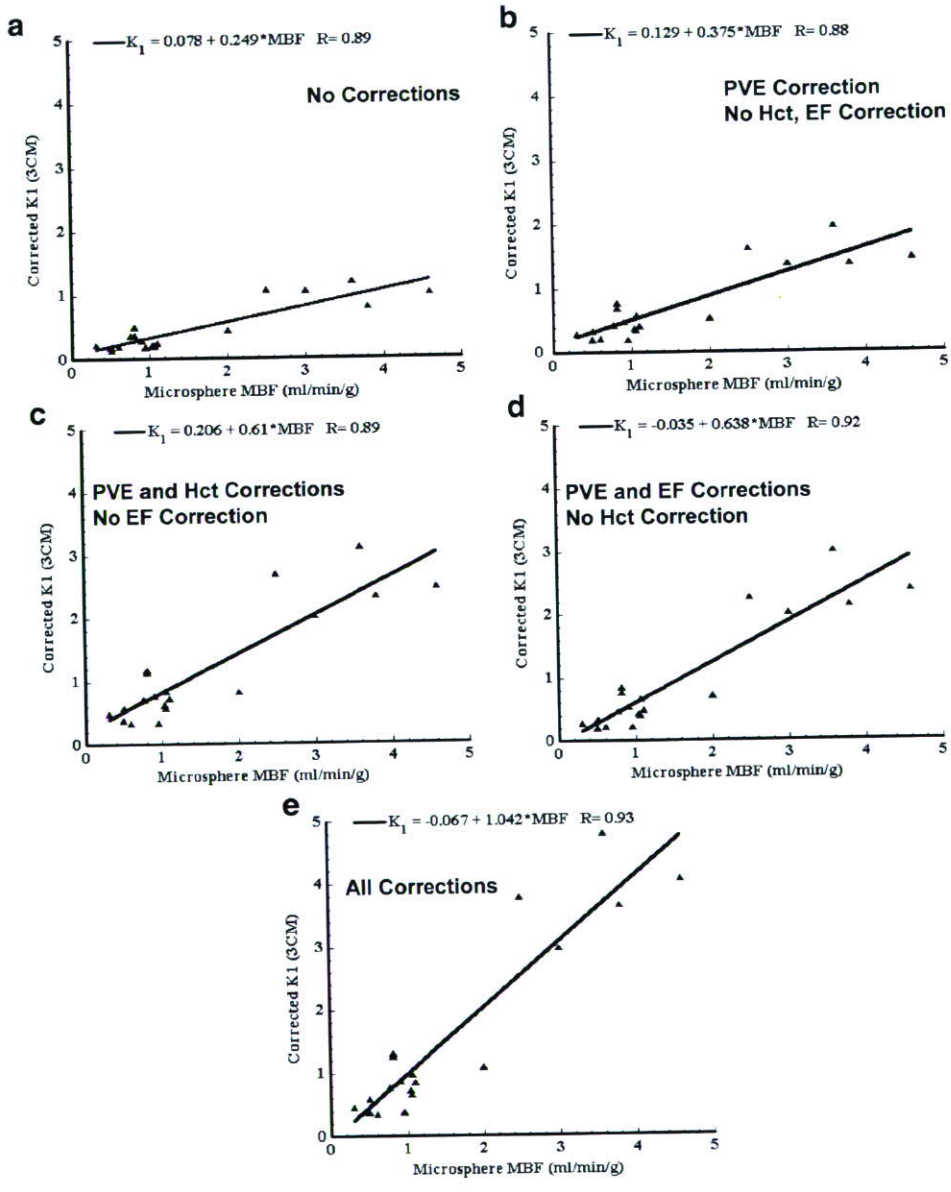

Fig. 6 Plot of K_1 derived from the three-compartment model fit against the mean of the pre- and post-dynamic SPECT microsphere blood flow measurements. **a** No correction for PVE, limited first-pass EF or conversion from plasma to blood flow has been applied. **b** Correction for PVE has been applied, but not for Hct or limited first-pass EF. **c** Corrections for PVE and Hct have been applied, but not for limited first-pass EF. **d** Corrections for PVE and limited first-pass EF have been applied, but not for Hct. **e** All corrections are applied for PVE, limited first-pass EF and Hct

Table 1 Summary of improvement in fit with the three-compartment model over the two-compartment model

Study group	Number of curves	Mean AIC two-compartment	Mean AIC three-compartment	Mean SC two-compartment	Mean SC three-compartment	Number of curves (%) (three-compartment better than two-compartment)[a]
Resting	35	652.4	630.2 ($p<0.01$)	663.8	638.4 ($p<0.01$)	24 (69)
Beta-blocker	20	378.4	378.8 (p=n.s.)	382.0 ($p<0.01$)	384.7	3 (15)
Adenosine	45	405.1	393.6 ($p<0.01$)	408.7	399.5 ($p<0.01$)	28 (62)

The p value indicates that the value in the cell is significantly lower than the corresponding other value.
AIC: Akaike information criterion, *SC*: Schwarz criterion
[a] This column gives the number of TTAC fits where the three-compartment model fit provided a significant improvement over the two-compartment fit according to all criteria (AIC, SC).

AIC and SC demonstrated that the three-compartment model fit provided significant improvement over the two-compartment model fit for resting and adenosine studies. For the beta-blocker studies, AIC between the two model fits was not significantly different, whilst SC demonstrated significantly better fit with the two-compartment model. Improved AIC and SC for the three-compartment model fit were observed in 69% of resting TTACs and 62% of adenosine TTACs, but only 15% in beta-blocker TTACs.

As shown in Fig. 7a and b, the K_1 and V_d values derived from the two-compartment model fit showed significant differences compared with those by the three-compartment model. Both K_1 and V_d were under-estimated with the two-compartment model fit compared with the three-compartment model fit. It should, however, be noted that there was a good correlation between the two- and three-compartment models for K_1, thus the bias introduced by the two-compartment model fit can potentially be corrected. K_1 values by the three-compartment model fit with all three corrections were 0.86±0.36, 2.71±1.64 and 0.55±0.24 ml/min/g corresponding to rest, adenosine infusion (with constant infusion at 140–700 mg/kg/h) and beta-blocker (with 2–6 mg administration), respectively. Difference in V_d was less than 10% and again this bias can potentially be corrected by the regression equation. The K_1 obtained with the two-compartment model also demonstrated a good correlation with the microsphere flow (Fig. 7c), though there was again a systematic under-estimation in K_1.

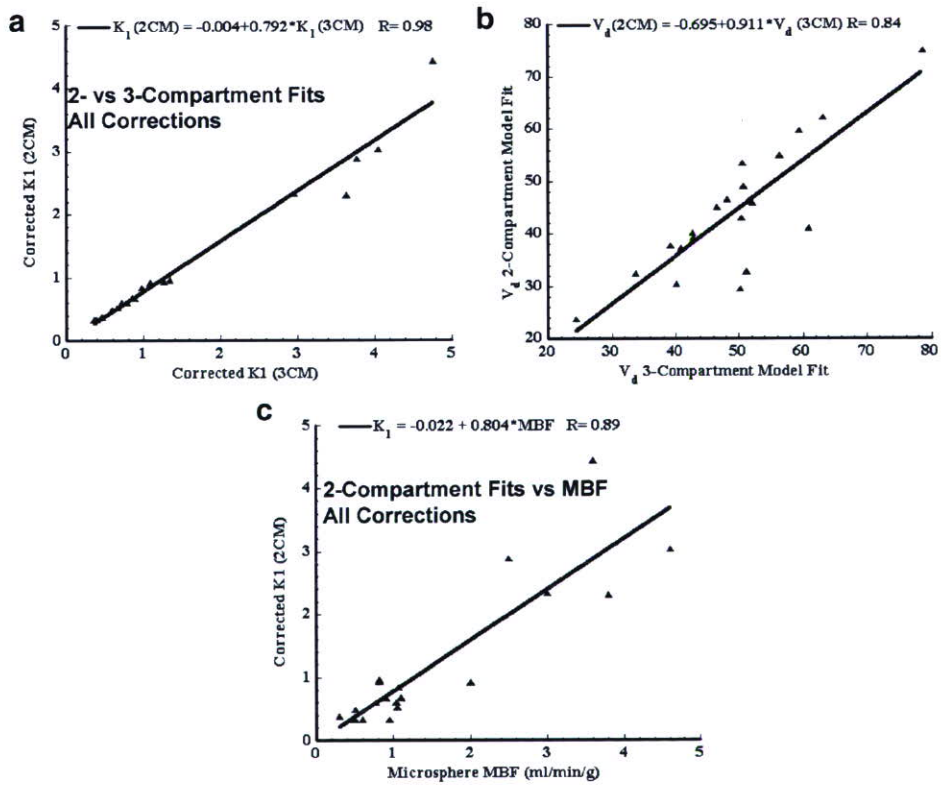

Fig. 7 **a** Plot of K_1 estimates derived from the two-compartment model fit against those from the three-compartment model fit. **b** Plot of V_d estimates derived from the two-compartment model fit against those from the three-compartment model fit. **c** Plot of K_1 values derived from the two-compartment model fit against mean of the pre- and post-dynamic SPECT microsphere blood flow measurements

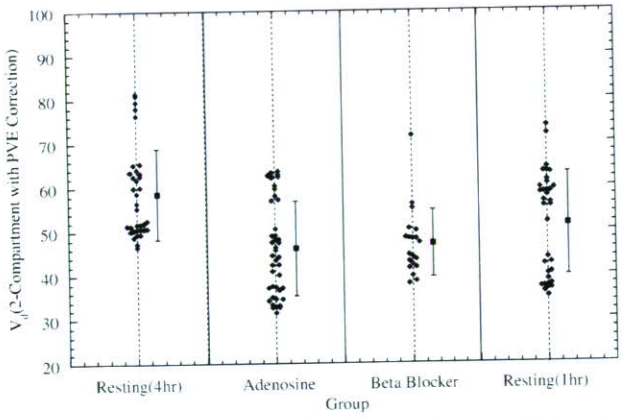

Fig. 8 V_d values obtained from the two-compartment model fit to the full 4 h resting data, adenosine and beta-blocker infusion 1 h curves and fit to first 1 h only of the resting study curves. Data from the multiple individual myocardial regions are shown

Figure 8 plots the V_d values for all evaluated myocardial segments for the fit to 4 h resting data, adenosine and beta-blocker infusion 1 h data and fit to only the first 1 h of resting data. The 4-h resting V_d values are significantly higher ($p<0.01$) compared with the adenosine, beta-blocker values and compared with the fit to the first 1 h resting data. However, the 1-h resting values are not significantly different from the beta-blocker V_d values nor the adenosine values.

Discussion

This study demonstrates that the kinetic analysis of quantitatively assessed myocardial ^{201}Tl accumulation (build-up and washout in healthy canines) provided quantitative MBF values, which agreed well with flows obtained using microspheres for a wide physiological range of flows. The size of the TTACs relative to the arterial plasma concentration corresponded well to the pharmacological stresses induced by adenosine and beta-blocker challenges. The compartmental model approach could reproduce these TTACs to make the determination of kinetic parameters, such as K_1 and V_d, possible. The three-compartment model gave results which were generally higher than the two-compartment model and which were statistically significantly better in terms of AIC, SC for the resting and adenosine studies, and this was in line with the visual inspection of the TTAC model fit curves. It should, however, be noted that the differences were only small between the two- and three-compartment model approaches, approximately 20% for K_1 and 10% for V_d The bias associated with the two-compartment model could be corrected by a linear regression as shown in Fig. 7a–c. This opens the possibility of using the more reliable two-compartment model fit due to its reduced number of parameters for routine clinical studies. The improved reliability of the two-compartment model fit in the clinical setting is particularly important if one intends to shorten the study time or generate parametric images.

The three corrections for PVE, Hct and first-pass EF proved to be important. The PVE correction method used in this work cannot, however, be applied to clinical studies, and the PVE correction in the beating heart still remains a considerable challenge in clinical studies. PVE may be reduced by gating the data, which may not, however, be feasible for the already noisy and large dynamic SPECT data sets. PVE may also be reduced by including resolution recovery as part of the reconstruction process [17–20]. Alternatively, it may also be possible to include PVE as part of the kinetic model fitting [21–25]. However, this adds extra fitting parameters and requires some parameters to be assumed fixed.

The input function is an important component in compartment model fitting. In this study, rapid arterial blood sampling was performed, and the plasma was separated by centrifugation. A number of important insights were gained by performing rapid separation of plasma in a subset of samples and dogs. It was found that ^{201}Tl enters the red blood cells as observed from the rapid separation of plasma in a subset of samples and dogs, which is not un-expected as potassium is also known [22] to be taken up by the red blood cells. The exchange of ^{201}Tl between red blood cells and plasma is relatively slow compared to the passage of blood through the capillary bed and hence direct uptake of activity from the red blood cells into tissue is believed to be negligible. Hence, tissue uptake will be dominated by the activity in the plasma during passage through the capillary bed and plasma in the substrate being measured. As a consequence, the flow measurement obtained with ^{201}Tl is plasma flow, which is in contrast to the microsphere studies, which measure whole blood flow. Conversion of plasma to blood flow was achieved by dividing the plasma flow by (1−Hct), as shown in Eq. 1, which then allowed the direct comparison with the microsphere measurements.

Rigorous estimation of the input function requires frequent arterial blood sampling. This is not only considered invasive, but also labor intensive. In addition, it has been shown in this study that rapid separation of the plasma for at least the first 30–40 min post-^{201}Tl administration is required to obtain accurate plasma concentration. If the separation of plasma is delayed, then the true plasma concentration at the time of sampling cannot be measured, which results in biased K_1 estimates. An empirical relationship of plasma to whole blood ratio as a function of time was developed and was found to be sufficiently consistent between dogs (Fig. 3) to allow the mean curve to be applied with minimal bias. Thus, in clinical practice, whole blood samples may be counted and converted to plasma concentration using the empirical relationship. This also potentially allows the input function to be obtained

non-invasively from the SPECT data using, for example, a curve derived from a left ventricular region. However, it should be noted that the relationship between plasma and whole blood counts in this study was derived for a 4-min infusion protocol and may be different for other injection protocols, such as bolus injection. Previously, it has been shown that population-based input functions calibrated with one or two blood samples could avoid the need for frequent arterial blood samples [26–28]. There is also a potential for applying this approach to ^{201}Tl studies. This is beyond the scope of this study and a systematic study should be designed to confirm this in clinical settings.

^{201}Tl has a high trans-capillary EF and thus the initial regional uptake of this tracer predominantly reflects the regional blood flow [10]. Use of a tracer that has a high first-pass EF is essential when one intends to quantitatively assess MBF at a high flow range or the coronary flow reserve. The EF of ^{201}Tl is reported as >0.8 [10] for a wide flow range and is known to be higher than ^{99m}Tc-labelled tracers such as tetrofosmine and sestamibi [29]. The physical characteristics of ^{201}Tl are unfortunately not ideal as low energy emission increases the attenuation factor and the scatter in the image. In addition, the relatively long half-life limits the administered activity to about a tenth of that with ^{99m}Tc tracers. Despite these shortcomings, the physiological characteristics of having high first-pass EF make ^{201}Tl an interesting tracer particularly for the absolute quantitation of MBF and the coronary flow reserve. This study demonstrates that quantitative physiological parameters can be derived from dynamic ^{201}Tl SPECT studies, despite its less than ideal imaging characteristics.

Whilst the quantitative physiological parameter estimation removed the systematic bias between MBF estimated by ^{201}Tl dynamic SPECT and by microspheres, the spread of data points around the regression line was rather large (Figs. 6e and 7c). This is not only due to possible errors in the estimation of MBF from the ^{201}Tl, but there was also considerable variation in flow estimated by the microspheres at the beginning and end of the study. Thus, at least part of the variability is attributable to errors in microsphere flow measurement, and particularly for the pharmaceutical intervention studies, flow may not have remained constant throughout the entire study duration, which may also account for some of the differences seen between the various flow measurements.

V_d estimated in this study could serve as an index of viability, as viable myocytes are required to maintain the large concentration gradient between plasma and myocardium at equilibrium. There was no significant difference in V_d values between rest, beta-blocker and adenosine studies when fitted for 1 h (Fig. 8). The significant difference between the 1- and 4-h fit for resting data could be explained by the limitation of the two-compartment model. Considerable spread in the V_d values observed over all dog studies on the other hand was partially attributed to the short (insufficient) scan time for reliable estimates of V_d. With the exception of the large, outlying V_d values in all 5 regions of 1 dog, the resting V_d values fell within a relatively narrow range of 47 to 65 (mean±SD=55±6). Given the sufficiently long scan time, significant reduction in V_d in infarcted areas may be detected. However, this would need to be tested with a suitable study design.

The scan time of 4 h required to achieve reliable V_d estimates is not practical in the routine clinical setting. As has been shown by Lau et al. [30], the scan period may be split into two sessions, an early dynamic scan for 30 min followed by a single static scan at approximately 3 h. This scheme is not more onerous than current rest/re-distribution protocols and hence could be practical. In addition, it may be possible to simplify the scanning protocol further to two static scans by using the table look-up method for the two-compartment model, which has been successfully employed for other SPECT tracers with relatively slow kinetics similar to ^{201}Tl [27, 31, 32]. This warrants further investigation.

This study relies on established, rigorous attenuation and scatter correction in SPECT [5] and availability of multi-detector SPECT systems capable of performing dynamic acquisition. To our knowledge, this is the first report that has demonstrated that it is possible to obtain quantitative physiological parameter estimates of K_1 and V_d in the myocardium using a clinical SPECT scanner and ^{201}Tl. This work suggests that it is feasible to apply our technique to clinical studies. Further studies are, however, needed to validate the proposed approach in the clinical setting. Incomplete motion correction is one possible error source, particularly in patients. Dynamic SPECT is probably more sensitive to the possible movement of patients during the study. Shortened clinical protocol is preferred, but this requires additional development to improve the reliability of parameter estimates. In addition, two scanning sessions are needed to assess the coronary flow reserve. We have recently demonstrated a technique to assess two cerebral blood flow images, one at rest and another after a vasodilating drug, from a single session of a SPECT scan in conjunction with split dose administration of ^{123}I-iodoamphetamine and dynamic SPECT [7]. As a clinical implication, the quantitative assessment of MBF and coronary flow reserve is important. For instance, coronary micro-vascular dysfunction or impaired endothelial function in patients with coronary risk factors or patients with cardiomyopathy or with heart failure is an un-resolved important issue to answer [11]. Coronary flow reserve can be reduced in patients with hypercholesterolemia without overt coronary stenosis [12]. A systematic study should be carried out to validate this approach for assessing MBF at rest and after adenosine from a single session of a scan.

Acknowledgement This study was supported by the Budget for Nuclear Research of the Ministry of Education, Culture, Sports, and Technology (MEXT), Japan; a grant from the Cooperative Link of Unique Science and Technology for Economy Revitalization promoted by the Ministry of Education, Culture, Sports and Technology, Japan and a grant for translational research from the Ministry of Health, Labour and Welfare (MHLW), Japan. We would like to thank Nihon Medi-Physics, Hyogo, Japan for providing the ^{201}Tl samples and also Mr. Yoshihide Takatani for his invaluable suggestion on the study design.

References

1. Gullberg GT, Huesman RH, Ross SG, et al. Dynamic cardiac single-photon emission computed tomography. In: Beller GA, Zaret BL, editors. Nuclear cardiology: state of the art and future directions. Philadelphia, PA: Mosby-Year Book Inc.; 1998. p. 137–87.
2. Chiao PC, Ficaro EP, Dayanikli F, Rogers WL, Schwaiger M. Compartmental analysis of technetium-99m-teboroxime kinetics employing fast dynamic SPECT at rest and stress. J Nucl Med 1994;35(8):1265–73.
3. Narita Y, Eberl S, Iida H, Hutton BF, Braun M, Nakamura T, et al. Monte Carlo and experimental evaluation of accuracy and noise properties of two scatter correction methods for SPECT. Phys Med Biol 1996;41(11):2481–96.
4. Narita Y, Iida H, Eberl S, Nakamura T. Monte Carlo evaluation of accuracy and noise properties of two scatter correction methods for ^{201}Tl cardiac SPECT. IEEE Trans Nucl Sci 1997;44:2465–72.
5. Iida H, Shoji Y, Sugawara S, Kinoshita T, Tamura Y, Narita Y, et al. Design and experimental validation of a quantitative myocardial ^{201}Tl SPECT System. IEEE Trans Nucl Sci 1999;46:720–6.
6. Iida H, Narita Y, Kado H, Kashikura A, Sugawara S, Shoji Y, et al. Effects of scatter and attenuation correction on quantitative assessment of regional cerebral blood flow with SPECT. J Nucl Med 1998;39(1):181–9.
7. Kim KM, Watabe H, Hayashi T, Hayashida K, Katafuchi T, Enomoto N, et al. Quantitative mapping of basal and vasareactive cerebral blood flow using split-dose ^{123}I-iodoamphetamine and single photon emission computed tomography. Neuroimage 2006;33(4):1126–35.
8. Beller GA, Watson DD, Pohost GM. Kinetics of thallium distribution and redistribution: clinical applications in sequential myocardial imaging. In: Pitt B, Strauss HW, editors. Cardiovascualar nuclear medicine. St. Louis: Mosby; 1979. p 225–42.
9. Berman DS, Maddhi J, Garcia EV. Role of thallium-201 imaging in the diagnosis of myocardial ischemia and infarction. In: F HS, editor. Nuclear medicine annual. New York: Raven; 1980. p 1–55.
10. Weich HF, Strauss HW, Pitt B. The extraction of thallium-201 by the myocardium. Circulation 1977;56(2):188–91.
11. Camici PG, Crea F. Coronary microvascular dysfunction. N Engl J Med 2007;356(8):830–40.
12. Yokoyama I, Ohtake T, Momomura S, Nishikawa J, Sasaki Y, Omata M. Reduced coronary flow reserve in hypercholesterolemic patients without overt coronary stenosis. Circulation 1996;94 (12):3232–8.
13. Li J, Tsuji BMW, Welch A, Frey EC, Gullberg GT. Energy window optimization in simultaneous Technetium-99m and Thallium-201 SPECT data acquisition. IEEE Trans Nucl Sci 1995;42:1207–13.
14. Meikle SR, Hutton BF, Bailey DL. A transmission-dependent method for scatter correction in SPECT. J Nucl Med 1994;35(2):360–7.
15. Hudson HM, Larkin RS. Accelerated image reconstruction using srdered subsets of projection data. IEEE Trans Med Imag 1994;13:601–9.
16. Choi Y, Hawkins RA, Huang SC, Brunken RC, Hoh CK, Messa C, et al. Evaluation of the effect of glucose ingestion and kinetic model configurations of FDG in the normal liver. J Nucl Med 1994;35(5):818–23.
17. Hutton BF, Hudson HM, Beekman FJ. A clinical perspective of accelerated statistical reconstruction. Eur J Nucl Med 1997;24 (7):797–808.
18. Hutton BF, Lau YH. Application of distance-dependent resolution compensation and post-reconstruction filtering for myocardial SPECT. Phys Med Biol 1998;43(6):1679–93.
19. Pretorius PH, King MA, Pan TS, de Vries DJ, Glick SJ, Byrne CL. Reducing the influence of the partial volume effect on SPECT activity quantitation with 3D modelling of spatial resolution in iterative reconstruction. Phys Med Biol 1998;43(2): 407–20.
20. Soares EJ, Glick SJ, King MA. Noise chaeacterization of combined Bellini-type attenuation correction and frequency-distance principle restoration filtering SPECT. IEEE Trans Nucl Sci 1996;43:3278–90.
21. Iida H, Kanno I, Takahashi A, Miura S, Murakami M, Takahashi K, et al. Measurement of absolute myocardial blood flow with H215O and dynamic positron-emission tomography. Strategy for quantification in relation to the partial-volume effect. Circulation 1988;78(1):104–15.
22. Araujo LI, Lammertsma AA, Rhodes CG, McFalls EO, Iida H, Rechavia E, et al. Noninvasive quantification of regional myocardial blood flow in coronary artery disease with oxygen-15-labeled carbon dioxide inhalation and positron emission tomography. Circulation 1991;83(3):875–85.
23. Bergmann SR, Herrero P, Markham J, Weinheimer CJ, Walsh MN. Noninvasive quantitation of myocardial blood flow in human subjects with oxygen-15-labeled water and positron emission tomography. J Am Coll Cardiol 1989;14(3):639–52.
24. Iida H, Rhodes CG, de Silva R, Yamamoto Y, Araujo LI, Maseri A, et al. Myocardial tissue fraction-correction for partial volume effects and measure of tissue viability. J Nucl Med 1991;32(11): 2169–75.
25. Iida H, Tamura Y, Kitamura K, Bloomfield PM, Eberl S, Ono Y. Histochemical correlates of (15)O-water-perfusable tissue fraction in experimental canine studies of old myocardial infarction. J Nucl Med 2000;41(10):1737–45.
26. Iida H, Itoh H, Nakazawa M, Hatazawa J, Nishimura H, Onishi Y, et al. Quantitative mapping of regional cerebral blood flow using iodine-123-IMP and SPECT. J Nucl Med 1994;35(12):2019–30.
27. Onishi Y, Yonekura Y, Nishizawa S, Tanaka F, Okazawa H, Ishizu K, et al. Noninvasive quantification of iodine-123-iomazenil SPECT. J Nucl Med 1996;37(2):374–8.
28. Takikawa S, Dhawan V, Spetsieris P, Robeson W, Chaly T, Dahl R, et al. Noninvasive quantitative fluorodeoxyglucose PET studies with an estimated input function derived from a population-based arterial blood curve. Radiology 1993;188(1):131–6.
29. Fukushima K, Momose M, Kondo C, Kusakabe K, Kasanuki H. Myocardial kinetics of (201)Thallium, (99m)Tc-tetrofosmin, and (99m)Tc-sestamibi in an acute ischemia–reperfusion model using isolated rat heart. Ann Nucl Med 2007;21(5):267–73.
30. Lau CH, Eberl S, Feng D, Iida H, Lun PK, Siu WC, et al. Optimized acquisition time and image sampling for dynamic SPECT of Tl-201. IEEE Trans Med Imag 1998;17(3): 334–43.
31. Iida H, Itoh H, Bloomfield PM, Munaka M, Higano S, Murakami M, et al. A method to quantitate cerebral blood flow using a rotating gamma camera and iodine-123 iodoamphetamine with one blood sampling. Eur J Nucl Med 1994;21(10):1072–84.
32. Onishi Y, Yonekura Y, Mukai T, Nishizawa S, Tanaka F, Okazawa H, et al. Simple quantification of benzodiazepine receptor binding and ligand transport using iodine-123-iomazenil and two SPECT scans. J Nucl Med 1995;36(7):1201–10.

ARTICLE IN PRESS
PSYN-09243; No of Pages 13
MODEL

Available online at www.sciencedirect.com
ScienceDirect
ELSEVIER
Psychiatry Research: Neuroimaging xx (2007) xxx – xxx
PSYCHIATRY RESEARCH NEUROIMAGING
www.elsevier.com/locate/psychresns

Progressive changes of white matter integrity in schizophrenia revealed by diffusion tensor imaging

Takeyuki Mori[a,b,c,1,2], Takashi Ohnishi[a,b,*,1], Ryota Hashimoto[b,e,f,1,3], Kiyotaka Nemoto[a,1], Yoshiya Moriguchi[a,1], Hiroko Noguchi[b,1], Tetsuo Nakabayashi[b,d,1], Hiroaki Hori[b,1], Seichi Harada[d,1], Osamu Saitoh[d,1], Hiroshi Matsuda[a,c,1,2], Hiroshi Kunugi[b,1]

[a]*Department of Radiology, National Center Hospital for Mental, Nervous, and Muscular Disorders, National Center of Neurology and Psychiatry, 4-1-1 Ogawa Higashi, Kodaira City, Tokyo, 187-8551, Japan*
[b]*Department of Mental Disorder Research, National Institute of Neuroscience, National Center of Neurology and Psychiatry, 4-1-1 Ogawa Higashi, Kodaira City, Tokyo, 187-8551, Japan*
[c]*Department of Nuclear Medicine, Saitama Medical School Hospital, 38 Morohongo Moroyama-machi, Iruma-gun, Saitama, 350-0495, Japan*
[d]*Department of Psychiatry, National Center Hospital for Mental, Nervous, and Muscular Disorders, National Center of Neurology and Psychiatry, 4-1-1 Ogawa Higashi, Kodaira City, Tokyo, 187-8551, Japan*
[e]*The Osaka-Hamamatsu Joint Research Center For Child Mental Development, Osaka University Graduate School of Medicine*
[f]*Department of Psychiatry, Osaka University Graduate School of Medicine*

Received 16 March 2006; received in revised form 6 July 2006; accepted 11 September 2006

Abstract

Recent magnetic resonance imaging (MRI) studies using diffusion tensor imaging (DTI) have suggested reduced fractional anisotropy (FA) in the white matter (WM) of the brain in patients with schizophrenia. We tried to examine whether such reduction in FA exists and whether such changes in FA progress in an age-dependent manner in a Japanese sample of chronic schizophrenia. FA values were compared between 42 patients with chronic schizophrenia and 42 controls matched for age and gender, by using DTI with voxel-by-voxel and region-of-interest analyses. Correlations of FA values with age and duration of illness were examined. Patients with schizophrenia showed lower FA values, compared to controls, in the widespread WM areas including the uncinate fasciculi and cingulum bundles. A significant group-by-age interaction was found for FA in the WM, i.e., age-related reduction of FA was more pronounced in schizophrenics than in controls. A significant negative correlation between FA and duration of illness was also found in the WM. Our data confirmed decreased FA in schizophrenics, compared to controls in the widespread WM areas. Such decreased FA values in schizophrenia might be attributable, at least in part, to progressive changes after the onset of the illness.

Keywords: Magnetic resonance imaging (MRI); DTI; Fractional anisotropy (FA); Aging

* Corresponding author. Department of Radiology, National Center Hospital for Mental, Nervous, and Muscular Disorders, National Center of Neurology and Psychiatry, 4-1-1 Ogawa Higashi, Kodaira City, Tokyo, 187-8551, Japan. Tel.: +81 42 341 2711; fax: +81 42 346 1790.
E-mail address: tohnishi@hotmail.com (T. Ohnishi).
[1] Tel.: +81 42 341 2711.
[2] Tel: +81 49 276 1111.
[3] D3, 2-2, Yamadaoka, Suita City, Osaka, 565-0871, Japan. Tel.: +81 6 6879 3074.

0925-4927/$ - see front matter © 2006 Elsevier Ireland Ltd. All rights reserved.
doi:10.1016/j.pscychresns.2006.09.004

Please cite this article as: Takeyuki Mori et al., Progressive changes of white matter integrity in schizophrenia revealed by diffusion tensor imaging, Psychiatry Research: Neuroimaging (2007), doi:10.1016/j.pscychresns.2006.09.004

1. Introduction

Diffusion tensor imaging (DTI) (Basser et al., 1994), a newly developed method to estimate the white matter (WM) integrity, provides information about the diffusion of water in biological tissues. In the WM, water diffusion is highly anisotropic, with greater diffusion in the direction parallel to axonal tracts. Thus, diminished anisotropy of water diffusion has been proposed to reflect compromised WM integrity (Lim et al., 1999). Fractional anisotropy (FA) (Basser, 1995) is a quantitative measure of diffusion anisotropy acquired from DTI.

The normally aging brain exhibits an assortment of micro- and macroscopic changes in the WM as well as the cerebral cortex. Histological studies demonstrate a decrease in myelin density and in the number of myelinated fibers (Meier-Ruge et al., 1992). Postmortem brain (Meier-Ruge et al., 1992) and volumetric neuroimaging studies (Christiansen et al., 1994; Salat et al., 1999) have suggested that WM changes are more prominent than cortical changes with aging, at least during certain segments of the age span and in certain regions of the brain. For example, volume loss in prefrontal WM is disproportionately greater than that in prefrontal cortex with late aging {comparison of elderly adults aged 60–75 with those aged >85 years (Salat et al., 1999)}. Several DTI studies have demonstrated age-related reductions of WM anisotropy in the genu of the corpus callosum (Pfefferbaum et al., 2000b), anterior WM (Pfefferbaum et al., 2000a; O'Sullivan et al., 2001), periventricular WM (Nusbaum et al., 2001), and the prefrontal WM (Nusbaum et al., 2001; Pfefferbaum et al., 2005; Salat et al., 2005).

Regarding schizophrenia, impairments of the neural connectivity between certain cortical areas, such as frontal and temporal areas, have been implicated in the pathophysiology of the disease (Frith and Dolan, 1996; Andreasen et al., 1997; Bullmore et al., 1997). Indeed, volumetric magnetic resonance (MR) studies and pathological studies demonstrated abnormalities of the WM in schizophrenia (Miyakawa et al., 1972; Cannon et al., 1998; Davis et al., 2003; Ho et al., 2003; Uranova et al., 2004). Changes in WM integrity in schizophrenia has relevance to the neural disconnection model of the disorder and may provide a basis for focal abnormalities as well. Several previous DTI studies in chronic schizophrenia showed decrease of FA in schizophrenics mainly in the front-temporal white matter and corpus callosum (Buchsbaum et al., 1998; Lim et al., 1999; Agartz et al., 2001; Burns et al., 2003). Furthermore, FA decrease in patients with first episode schizophrenia might be less pronounced compared to chronic patients (Price et al., 2005; Szeszko et al., 2005), suggesting that the decreased FA in schizophrenics might be attributed, at least in part, to progressive and exaggerated age-dependent changes in schizophrenics rather than neurodevelopmental abnormalities in the WM. To date, there is only one cross-sectional study with a small sample size investigating age-related FA changes in schizophrenia that demonstrated an age-related FA increase in schizophrenics (Jones et al., 2006).

The present study was aimed to examine whether patients with chronic schizophrenia do have reduced FA values compared to controls and whether such changes in FA progress in an age-dependent manner.

2. Methods

2.1. Subjects

Table 1 shows the characteristics of participants of this study. Forty-two patients with chronic schizophrenia were recruited at the National Center of Neurology and Psychiatry, Tokyo, Japan. Consensus diagnosis was made for each patient by at least two trained psychiatrists according to the DSM-IV criteria (American Psychiatric Association, 1994), based on all available information, including clinical interviews, medical records and other research assessments. All patients were stable and/or partially remitted and had been taking antipsychotic medication at the time of MR measurement and neuropsychological tests. Forty-two healthy volunteers who had no current or past contact to any psychiatric services served as controls. All the subjects were biologically unrelated Japanese. After description of the study, written informed consent was obtained from every subject. The study protocol was approved by the ethics committee of the National Center of Neurology and Psychiatry, Tokyo, Japan. Exclusion criteria for all the participants included asymptomatic or symptomatic cerebral infarctions detected by T2 weighted MRI, serious neurological or endocrine disorder, any medical condition that could potentially affect the central nervous system, or mental retardation according to DSM-IV criteria.

2.2. Image acquisition

MR studies were performed on a 1.5 tesla Magnetom Vision Plus system (Siemens, Erlangen, Germany). Axial DTI scans aligned to the plane containing anterior and posterior commissures were acquired with a pulsed-

Please cite this article as: Takeyuki Mori et al., Progressive changes of white matter integrity in schizophrenia revealed by diffusion tensor imaging, Psychiatry Research: Neuroimaging (2007), doi:10.1016/j.pscychresns.2006.09.004

Table 1
Characteristics of participants

	Controls	Schizophrenics	Two sample *t*-test	(Two-tailed; df=82)
			t	*P*
Number of subjects	42	42		
Gender (male/female)	26/16	26/16		
Handedness (right/left)	41/1	41/1		
Age (years)	39.2 (9.0)	40.0 (9.3)	−0.42	0.68
Range of age (years)	22–59	22–59		
Education (years)	17.1 (3.5)	13.0 (2.9)	8.1	<0.001
Full-scale IQ (WAIS-R)	114.3 (11.6)	86.0 (21.3)	6.0	<0.001
Age of onset		23.3 (7.0)		
Duration of illness (years)		16.8 (9.0)		
Duration of hospitalization (months)		31.2 (61.3)		
Dose of total antipsychotic drugs (mg/day, chlorpromazine equivalent)		1005.1 (735.3)		
Dose of typical antipsychotic drugs (mg/day, chlorpromazine equivalent)		694.8 (748.3)		
Dose of atypical antipsychotic drugs (mg/day, chlorpromazine equivalent)		310.3 (464.2)		

Mean (S.D.).
WAIS-R: Wechsler Adult Intelligence Scale-Revised.

gradient, spin-echo, single-shot echo planar imaging (EPI) sequence (TR/TE=4000/100 ms; acquisition matrix, 256×256; NEX=4, FOV 240 mm; b=1000 s/mm^2; 20 slices, slice thickness 5 mm, gap 1.5 mm). Diffusion was measured along six non-collinear directions. For each of six gradient directions, four acquisitions were averaged. Four acquisitions without diffusion weighting (b=0) were also averaged. Additionally, a three dimensional volumetric acquisition of a T1-weighted gradient echo sequence with a gapless series of thin sagittal sections using an MPRage sequence (TR/TE=11.4/4.4 ms; flip angle, 15 degree; acquisition matrix, 256×256; NEX=1, FOV 315 mm; slice thickness 1.23 mm) was acquired for evaluating the volume of grey matter (GM), WM and cerebrospinal fluid (CSF) space.

2.3. Image processing

FA images for each subject were computed from seven diffusion images acquired as above by an in-house script on Matlab 6.5 software (Mathworks, Inc., MA, USA). Then, the FA images were spatially-normalized using high-dimensional-warping algorithm (Ashburner et al., 1999) and were matched to the FA template image. To make the FA template image, we warped FA images of 4 normal subjects (other than 42 control subjects) to the single-subject T1 template (skull stripped image) using spatial normalization function of SPM2 and averaged the 4 warped FA images. The transformed FA images were smoothed with a Gaussian kernel. The filter size (full-width at half-maximum: FWHM) was varied from zero to 16 mm in steps of 2 mm to validate the consistency of results of SPM analyses, because a previous study (Jones et al., 2005) reported that the statistical results of SPM analyses were differed depending on filter size. For measuring the volume of GM, WM and CSF space, an additional function of an optimized VBM script (http://dbm.neuro.uni-jena.de/vbm) was used (Good et al., 2001).

2.4. Statistical analysis

2.4.1. Voxel-by-voxel analysis

The resultant FA images were analyzed using statistical parametric mapping with the framework of the General Linear Model in SPM2 (Wellcome Department of Cognitive Neurology, London, UK) (Friston et al., 1995). We constituted following three

Table 2
The relationship between smoothing kernel sizes (FWHM) and number of resels in our sample

FWHM (mm)	Number of resels
None	12460.4
2×2×2	5131.1
4×4×4	1720.2
6×6×6	706.0
8×8×8	289.4
10×10×10	119.7
12×12×12	52.1
14×14×14	24.4
16×16×16	12.4

Please cite this article as: Takeyuki Mori et al., Progressive changes of white matter integrity in schizophrenia revealed by diffusion tensor imaging, Psychiatry Research: Neuroimaging (2007), doi:10.1016/j.pscychresns.2006.09.004

statistical analyses: 1) a two-sample *t*-test for estimating group differences (controls versus schizophrenics), 2) a correlational analysis between age and FA values in both controls and the schizophrenics and 3) a correlational analysis of FA values with duration of illness, age of onset, duration of hospitalization, and daily dose of

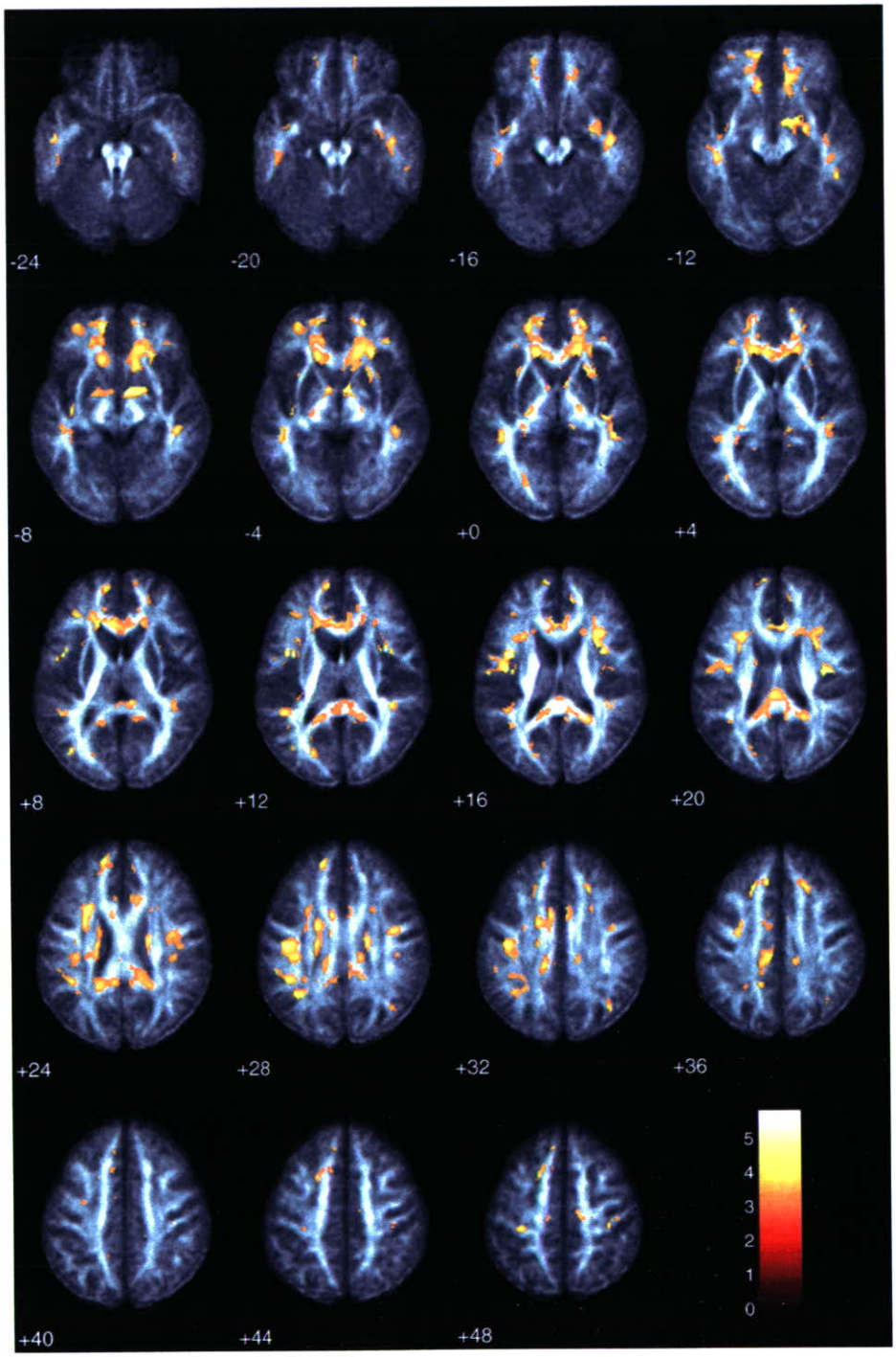

Fig. 1. Comparison in FA values between patients with schizophrenia and controls. The SPM {t} is displayed onto axial FA template images. The WM areas in which significantly lower FA values in patients compared with controls were observed, including the bilateral frontal and temporal WM, uncinate fasciculi, cingulum bundles, and genu and splenium of the corpus callosum ($P<0.001$, uncorrected).

Please cite this article as: Takeyuki Mori et al., Progressive changes of white matter integrity in schizophrenia revealed by diffusion tensor imaging, Psychiatry Research: Neuroimaging (2007), doi:10.1016/j.pscychresns.2006.09.004

antipsychotic drugs in the schizophrenics. In all the three analyses, relative WM volume (WM volume divided by the summation of GM, WM and CSF volumes) and WAIS-R (Wechsler Adult Intelligence Scale-Revised) full-scale IQ score were treated as nuisance variables. The former was included for eliminating the possible effect of WM volume change associated with aging on the FA values through partial voluming from non-WM voxels. The latter was included to allow for the effects of IQ, because there was some evidence which suggested DTI measures were correlated with cognitive decline in elderly (O'Sullivan et al., 2004). We additionally conducted the analyses without these two nuisance variables to check whether there were any differences in the results with or without nuisance variables in the statistical models. To estimate population effects (diagnostic effects), we used a single-subject, condition (controls or schizophrenics) and covariate (no covariate of interest) model for the SPM analysis. In the second analysis, we applied the single subject condition (controls or schizophrenics) and covariate (interaction with condition, covariate of interest; age) model. A single-subject, covariate only model was applied in the third analysis. For these three analyses, we set masking threshold for FA values of 0.2 for excluding voxels containing partial volume of WM and other tissues. Since the previous study demonstrating a positive correlation between FA values and age in schizophrenics reported mean FA values of around 0.4 (Jones et al., 2006), we additionally set masking threshold for FA values of 0.35 for examining correlation between age and FA values of more anisotropic WM structure in the second analysis. For the evaluation of the statistical models, we used Wake Forest University Pickatlas (Maldjian et al., 2003) to pick up cerebral WM in the Montreal Neurological Institute (MNI) space. We used uncorrected $P<0.001$ as a statistical threshold to search significant differences. As demonstrated in Table 2, the number of resels differed profoundly depending on smoothing kernel sizes (FWHM) and the statistical results with correction for multiple comparisons could change dramatically relying on number of resels. On the other hand, SPM results without correction for multiple comparisons were essentially unchanged regardless of smoothing kernel size (data not shown). Therefore, we did not perform correction for multiple comparisons. The resultant set of t values constituted statistical parametric map (SPM {t}). We employed the filter size of 6 mm for presentation of the results considering for the original voxel dimensions of acquired data {0.94 mm × 0.94 mm × (5.00 + 1.50) mm}.

2.4.2. ROI analysis

To ensure the robustness of the results of the voxel-by-voxel analyses, we additionally performed ROI analyses. We used MarsBar (http://marsbar.sourceforge.net/) for extracting region of interest (ROI) containing all the voxels classified as WM with Wake Forest University Pickatlas from spatially normalized and smoothed FA images and calculated mean FA values of the ROI. Then, we performed correlational analyses of mean FA values with the same variables in voxel-by-voxel analysis using Statistical Package for Social Science (SPSS), 1) in both controls and schizophrenics, 2) in controls and 3) in schizophrenics. We constituted a General Linear Model for the first analysis and entered diagnosis-by-age interaction effects into the statistical model to examine if there were any diagnosis-by-age interaction effects. For the second and third analyses, Pearson's correlation coefficients between mean WM FA values and covariates were calculated.

3. Results

3.1. Voxel-by-voxel analyses

3.1.1. Comparison between schizophrenics and controls

Schizophrenics demonstrated significantly lower FA values in widespread WM areas, compared with controls. These WM areas included bilateral frontal and temporal lobes, uncinate fasciculi (external capsules), cingulum bundles, and genu and splenium of corpus

Table 3
The summary of the WM areas in which significantly lower FA values in patients compared with controls were observed

Anatomical regions	t-value	MNI coordinates		
	(Voxel level)	x	y	z
Rt frontal lobe white matter	4.34	22.5	52.5	−4.5
Lt frontal lobe white matter	5.43	−13.5	49.5	−6
Rt temporal lobe white matter	4.25	48	−33	−7.5
Lt temporal lobe white matter	4.19	−45	−31.5	−10.5
Rt uncinate fasciculus (external capsule)	4.00	33	12	−1.5
Lt uncinate fasciculus (external capsule)	3.84	−33	12	−1.5
Rt cingulate bundle	4.23	6	6	33
Lt cingulate bundle	4.32	−7.5	6	30
genu of corpus callosum	3.79	6	24	10.5
splenium of corpus callosum	4.18	−3	−33	19.5

Please cite this article as: Takeyuki Mori et al., Progressive changes of white matter integrity in schizophrenia revealed by diffusion tensor imaging, Psychiatry Research: Neuroimaging (2007), doi:10.1016/j.pscychresns.2006.09.004

callosum (Fig. 1, Table 3). There would be increased possibility of alpha errors because we did not perform correction for multiple comparisons. However, our results were in well concordance with the results of the previous studies (Buchsbaum et al., 1998; Lim et al., 1999; Agartz et al., 2001; Burns et al., 2003; Kubicki

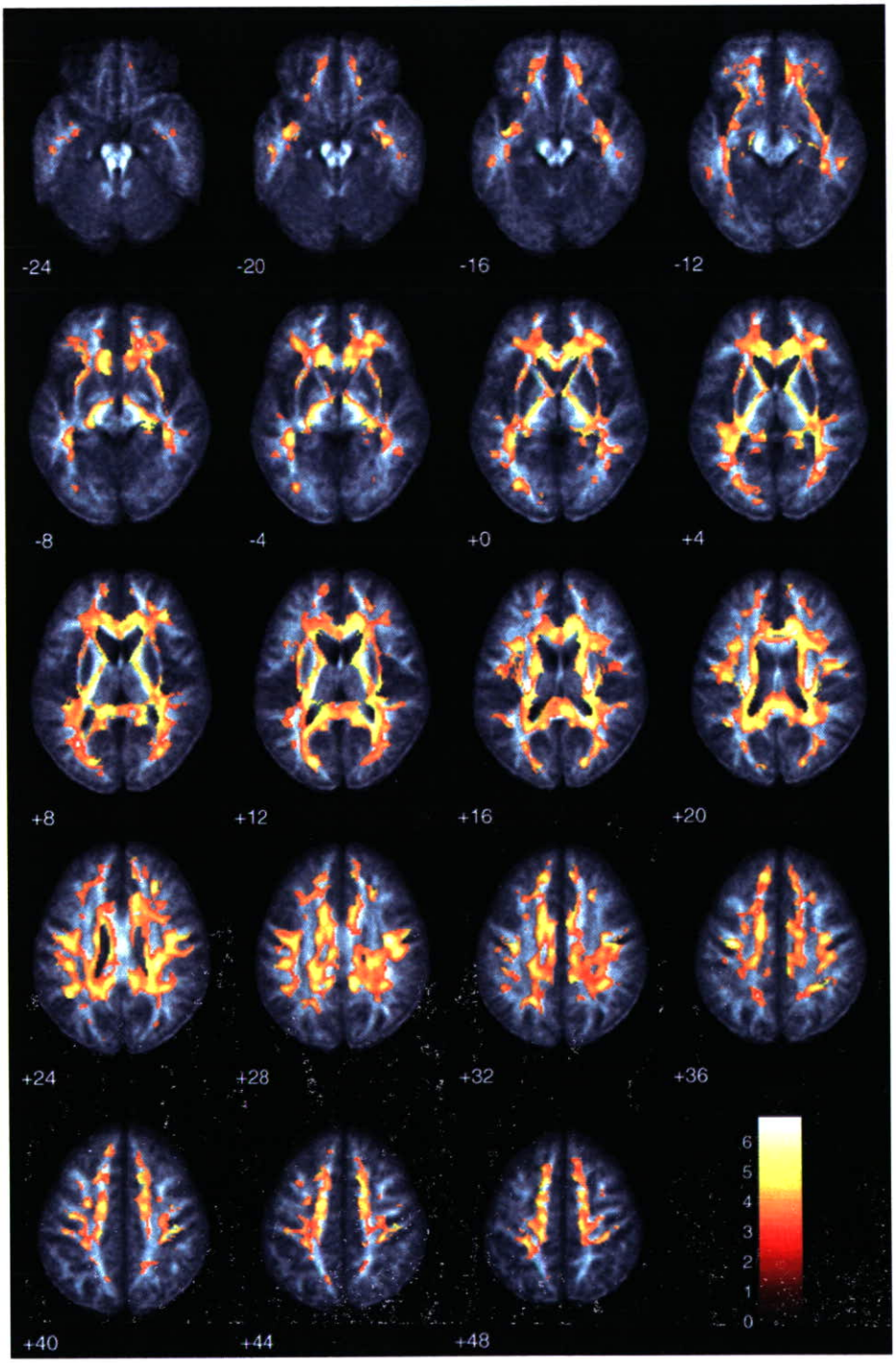

Fig. 2. Correlational analysis between FA values and age with 0.2 as a masking threshold in schizophrenics. The SPM {t} is displayed onto axial FA template images. The widespread WM areas showed a significant negative correlation between FA values and age in schizophrenics ($P<0.001$, uncorrected).

Please cite this article as: Takeyuki Mori et al., Progressive changes of white matter integrity in schizophrenia revealed by diffusion tensor imaging, Psychiatry Research: Neuroimaging (2007), doi:10.1016/j.pscychresns.2006.09.004

et al., 2003). Therefore, we might be able to regard the results of these previous studies as a priori hypotheses. There were no areas of significantly higher FA values in patients compared with controls even at a lenient threshold ($P<0.05$, uncorrected). In these results of the analysis without nuisance variables in the statistical

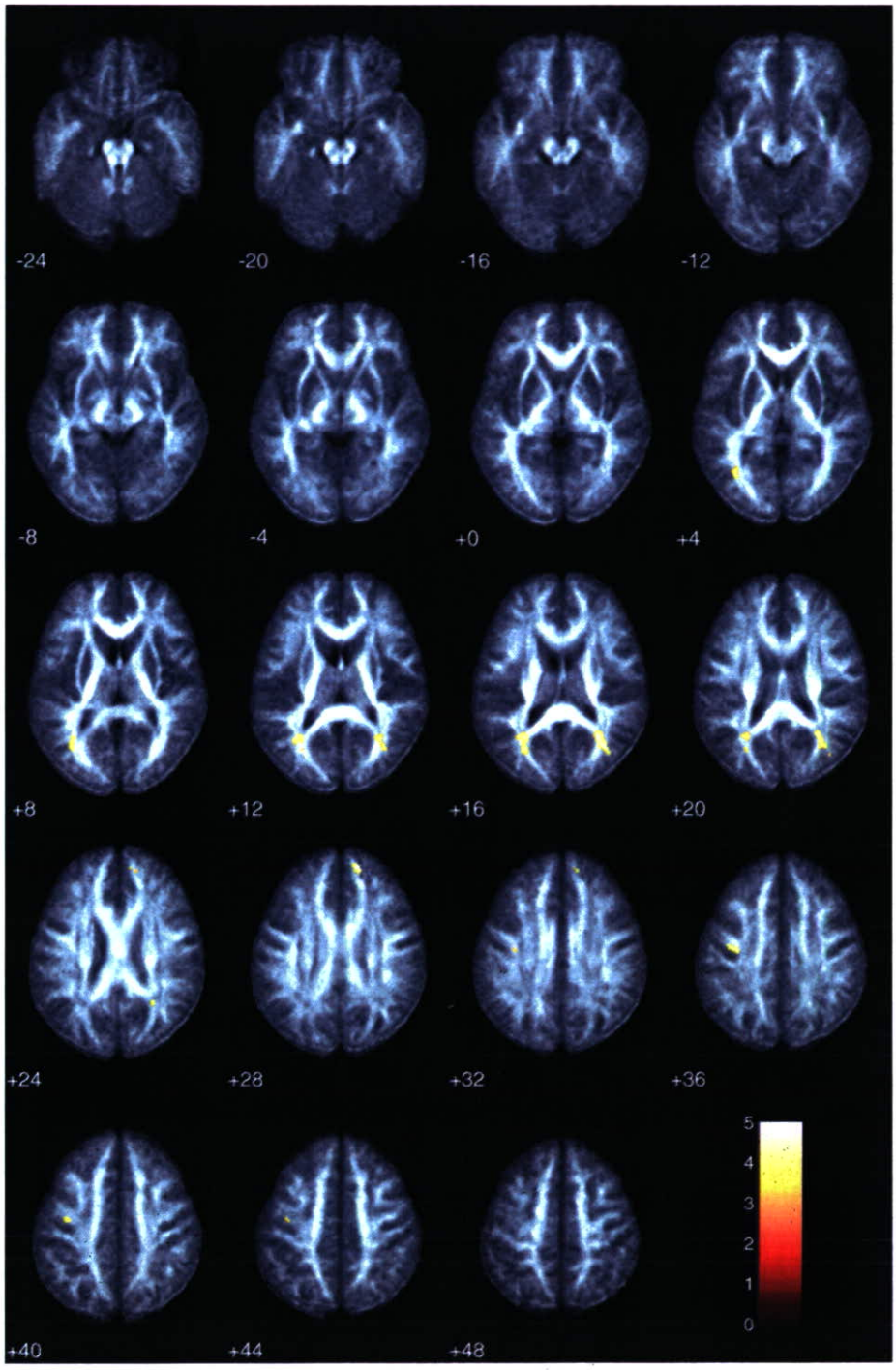

Fig. 3. Correlational analysis between FA values and age with 0.2 as a masking threshold in controls. The SPM {t} is displayed onto axial FA template images. The WM areas showed a significant negative correlation between FA values and age in controls ($P<0.001$, uncorrected), including right prefrontal {(15.0, 49.5, 30.0) in MNI coordinates, $t=5.03$}, left frontal {(−37.5, −15.0, 34.5), $t=4.51$} and bilateral temporo-occipital WM {(31.5, −60.0, 16.5), $t=4.75$; (−30.0, −60.0, 15.0), $t=4.47$}.

Please cite this article as: Takeyuki Mori et al., Progressive changes of white matter integrity in schizophrenia revealed by diffusion tensor imaging, Psychiatry Research: Neuroimaging (2007), doi:10.1016/j.pscychresns.2006.09.004

models, the distributions of the statistically significant areas were essentially unchanged compared to the results with nuisance variables although the spatial extents of the statistically significant areas were slightly larger (data not shown), which was the case with the results of other two analyses.

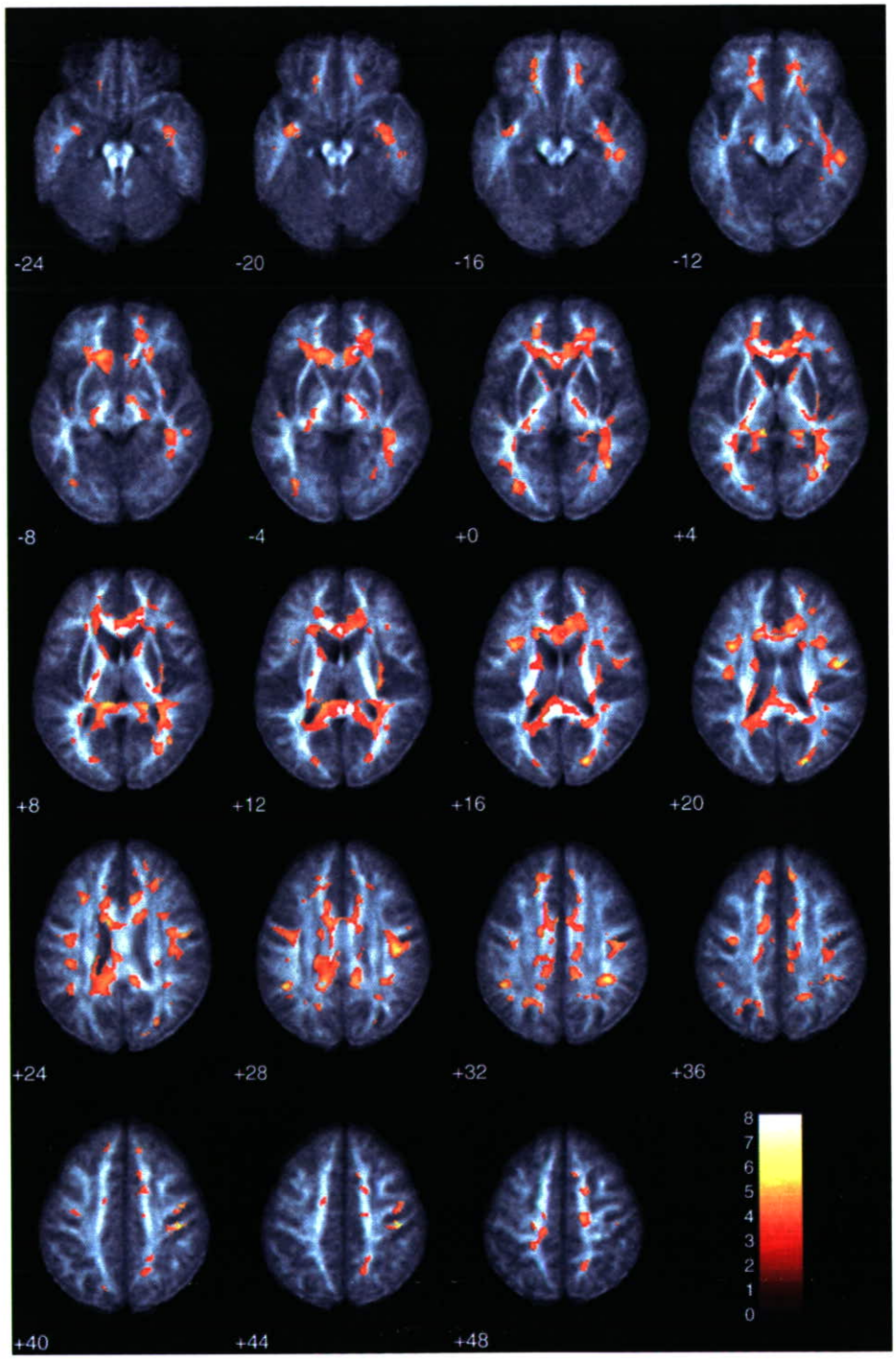

Fig. 4. Correlational analysis between FA values and duration of illness with 0.2 as a masking threshold in schizophrenics. The SPM {t} is displayed onto axial FA template images. The widespread WM areas showed a significant negative correlation between FA values and duration of illness in schizophrenics ($P<0.001$, uncorrected).

Please cite this article as: Takeyuki Mori et al., Progressive changes of white matter integrity in schizophrenia revealed by diffusion tensor imaging, Psychiatry Research: Neuroimaging (2007), doi:10.1016/j.pscychresns.2006.09.004

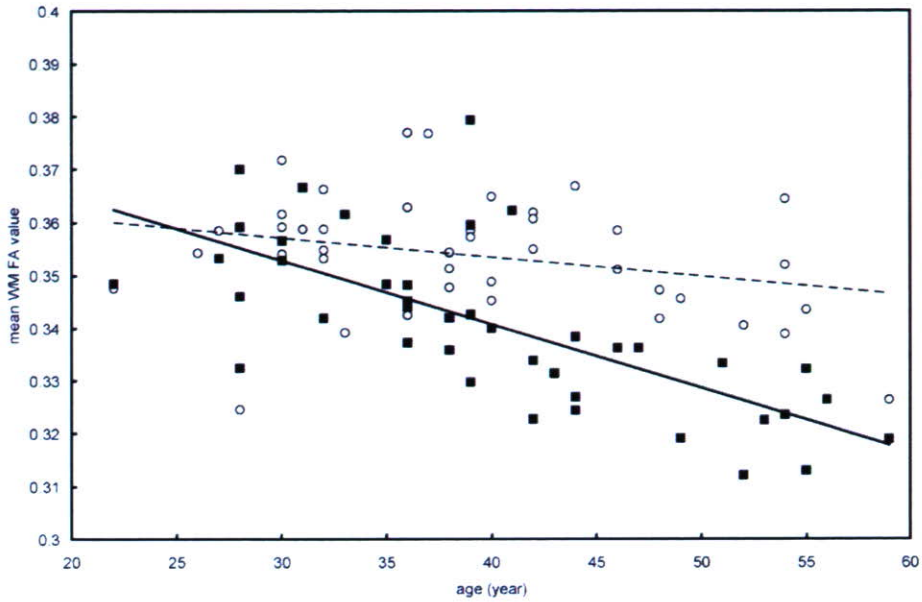

Fig. 5. A scatter plot between age and mean WM FA value when masking threshold for FA values was set to 0.2. Filled squares represent schizophrenics and open circles represent controls. The solid line indicates a regression line for schizophrenics ($y=-0.0012\times+0.3888$, $R^2=0.49$, test for regression slope: df=40; $t=-6.24$; $P<0.0001$). The dashed line indicates a regression line for controls ($y=-0.0004\times+0.3679$, $R^2=0.083$, test for regression slope: df=40; $t=-1.90$; $P=0.065$). A significant diagnosis-by-age interaction effect (general linear model: $P=0.009$) was noted.

3.1.2. Correlational analysis in schizophrenic and control groups

As the results of the second analysis considering aging effects, a significant negative correlation with age was observed in the FA values of widespread, almost diffuse WM areas in the schizophrenic group (Fig. 2), while in the control group, only FA values in right prefrontal {(15.0, 49.5, 30.0) in MNI coordinates, $t=5.03$}, left frontal {(−37.5, −15.0, 34.5), $t=4.51$} and bilateral temporo-occipital WM {(31.5, −60.0, 16.5), $t=4.75$;

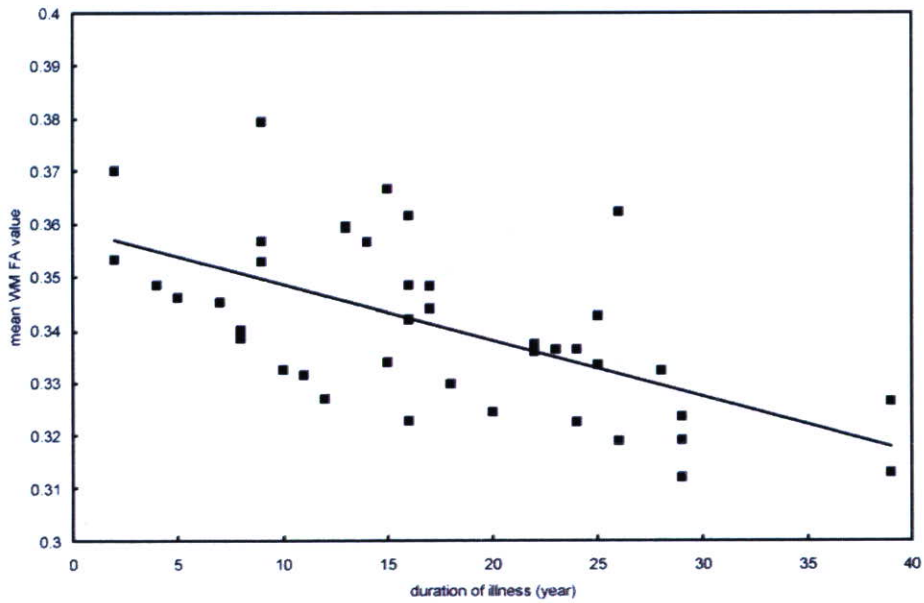

Fig. 6. A scatter plot between duration of illness and mean WM FA value when masking threshold for FA values was set to 0.2. Filled squares represent schizophrenics. The solid line indicates a regression line for schizophrenics ($y=-0.0011\times+0.3590$, $R^2=0.36$, test for regression slope: df=40; $t=-4.78$; $P<0.0001$).

Please cite this article as: Takeyuki Mori et al., Progressive changes of white matter integrity in schizophrenia revealed by diffusion tensor imaging, Psychiatry Research: Neuroimaging (2007), doi:10.1016/j.pscychresns.2006.09.004